Active Damping for Model Predictive Pulse Pattern Control

Peter Hokayem, Tobias Geyer, Nikolaos Oikonomou

ABB Corporate Research Center
Segelhofstrasse 1K, CH-5405 Baden-Dättwil, Aargau, Switzerland
Email: {peter.al-hokayem,tobias.geyer, nikolaos.oikonomou}@ch.abb.com

***Abstract*—This paper pertains to medium voltage converters that are equipped with an *LC* resonant output filter. We provide a new active damping method, based on Linear Quadratic Regulator (LQR) theory, for a converter running with a Model Predictive Pulse Pattern Controller. The new active damping method relies on filtered versions of all measured signals to compute corrective actions that are combined with the flux error signal. These corrective actions of the flux error successfully attenuate the resonant behavior caused by the output filter. The proposed method is validated via extensive simulation results.**

I. Introduction

Medium Voltage (MV) AC drives are the backbone of industrial applications, such as marine and mining. A general setup of MV drives is depicted in Figure 1, in which the AC to DC rectifier unit is connected to the grid via a transformer and is used to charge the DC capacitor bank. The Inverter Unit (INU) extracts power out of the DC bank to generate 3-phase switched voltage signals, which are in turn used to drive the AC machine. The INU is typically operated at low switching

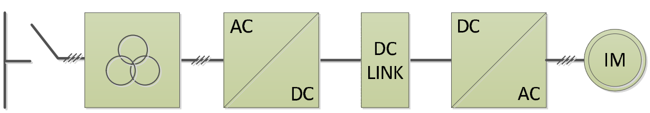

Fig. 1: Medium Voltage AC Drive

frequencies (especially at high load currents) in order to minimize switching losses. Moreover, the INU is required to drive the Induction Machine (IM) with a low current THD (Total Harmonic Distortion). These requirements necessarily impose some restrictions on the modulation scheme to be used. Optimized Pulse Patterns (OPPs) [1] do provide such low current THD requirement but are typically required to have certain smoothness of the switching angles over the modulation index, hence rendering the offline computation of the OPPs difficult and limiting the dynamic capability of the controller in closed-loop. Recently, an online OPP-based Model Predictive Pulse Pattern Control (MP^{3}C) method has been proposed [3]. MP^{3}C is a novel method to achieve fast closed-loop control of an AC machine with an *N*-level voltage source inverter [6], and which does not require smoothness of the switching angles over the modulation index. MP^{3}C relies on OPPs with low THD factors that are computed offline [1]. The OPPs are used to generate reference flux trajectories that are to be followed. The core of MP^{3}C is an online computational stage that adjusts the switching instants in the OPPs so as to maintain the flux on the reference trajectory in closed-loop.

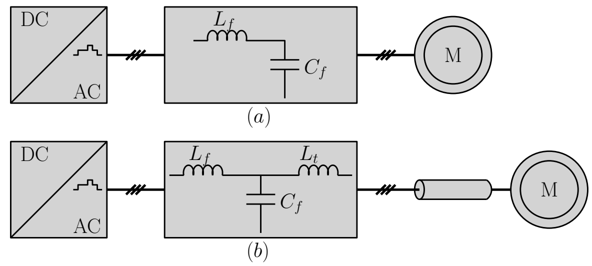

Fig. 2: (a) INU connected through an *LC* filter to the machine. (b) INU connected through an *LC* filter, step-up transformer, and long cable to the machine.

Instead of directly connecting the INU to the machine, one may opt for installing an extra *LC*-type filter between the INU and the machine in order to attenuate the harmonic content in the 3-phase stator current at higher frequencies. The drawback of such an approach is that the *LC* filter exhibits a certain resonant behavior that may result in instabilities if left untreated [7], [8].

In a setup with an *LC* filter, the main challenge is to ensure stability of the closed-loop system. The remedy is to provide the underlying control method (MP^{3}C in our case) with information regarding the content of the current/voltage signals around the resonant frequency and to allow the controller to react to such information in order to actively damp the filter-induced oscillations. This Active Damping (AD) problem arises in several scenarios pertaining to Power Electronic Converters, as shown in Figure 2.

Active damping for power electronic circuits with *LC* filters has been studied for various control methods. AD for Direct Torque Control (DTC) may be found in [7], [8]. AD for Model Predictive DTC (MPDTC) may be found in [5]. Finally, AD for Pulse Width Modulation (PWM) methods may be found, for example, in [2], [4]. Essentially, the main idea can be abstracted into the design of an outer loop that provides corrective actions (based on the harmonic content of the measure/reconstructed signals) to be fed into the various underlying controllers. The subject matter of this article is to combine MP^{3}C [3], an OPP-based control method, with an LQR-based AD loop that achieves the desired attenuation at the resonant peak of the system, consisting of the *LC* filter and the machine.

The remainder of this paper is organized as follows: Section II gives the problem formulation. Section III provides the new

978-1-4799-5776-7/14/$31.00 ©2014 IEEE

control method used for AD of MP3C. We give extensive simulation results in Section IV that validate our approach, and conclude this paper in Section V.

A. Notation

The main signals and parameters that are used throughout the paper are listed in Table I below. For any two dimensional vector $v \in \mathbb{R}^2$, let $\|v\|$ indicate its Euclidean norm and $\angle v$ indicate its angle in the xy-plane.

TABLE I: Signals and Parameters

Description	Symbol
Stator flux	ψ_s
Stator input voltage	v_s
Rotor flux	ψ_r
Rotational speed	ω
Electric torque	T
Load torque	T_l
Load angle (between ψ_s and ψ_r)	γ
Stator resistance	R_s
Rotor resistance	R_r
Stator inductance	L_s
Rotor inductance	L_r
Magnetizing inductance	L_m
Leakage factor	$\sigma = 1 - \frac{L_m^2}{L_s L_r}$
Inertia	J

II. Problem Formulation

A. Machine Model

Consider the setup in which an INU is driving an Induction Machine (IM) via an *LC* filter, as shown in Figure 3. The

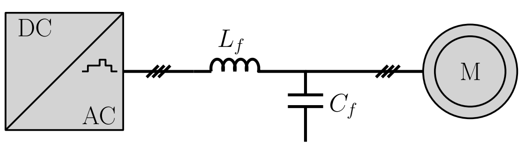

Fig. 3: INU connected through an *LC* filter to an induction machine

machine model is described via the standard equations in the xy-plane

$$\begin{aligned}
\frac{d\psi_s}{dt} &= u_s - \left(\frac{R_s}{\sigma L_s}\right)\psi_s - \left(\frac{R_s}{\sigma L_s}\right)\left(\frac{L_m}{L_r}\right)\psi_r \\
\frac{d\psi_r}{dt} &= \left(\frac{R_r}{\sigma L_r}\right)\left(\frac{L_m}{L_s}\right)\psi_s - \left(\frac{R_r}{\sigma L_r}\right)\psi_r + \omega\begin{bmatrix}0 & -1\\ 1 & 0\end{bmatrix}\psi_r \\
J\frac{d\omega}{dt} &= T - T_l \\
T &= \left(\frac{L_m}{L_s L_r - L_m^2}\right)\|\psi_s\|\,\|\psi_r\|\sin(\gamma)
\end{aligned}$$

where the signals and parameters are as listed in Table I. In case the *LC* filter is absent, then one would operate the INU output in order to generate v_s and operate the machine at some given speed ω^* by providing a certain torque T^*. This is done under the assumption that the output voltage of the inverter u_i is equal to the stator voltage u_s. In the presence of the *LC* filter, this latter fact does not hold and hence one requires an adaptation of the underlying control method.

B. LC Resonant Filter Properties

The INU operates in discrete voltage levels that are fractions of the full DC link voltage, resulting in harmonics at frequencies other than the fundamental frequency f_1. Hence, one may choose to add a resonant *LC* filter between the DC to AC converter and the machine in order to attenuate the unwanted harmonic content in the output currents. The

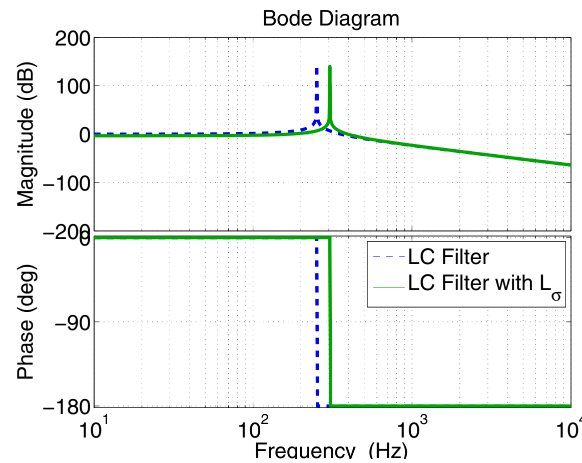

Fig. 4: Response of an *LC* filter without being connected to the machine (dashed blue) and the corresponding response when connected to the machine, which is modeled as the total leakage inductance L_σ (green). The behavior is virtually identical for both cases at high frequencies, and the presence of the machine contributes to shifting the resonant frequency from 252 Hz to 304 Hz.

resonant filter has a steep attenuation rate of the harmonic content beyond the resonant frequency; thus the harmonic content for very high frequencies is almost eliminated (see Figure 4). This positive effect is accompanied by a substantial magnification of the harmonic content around the resonant frequency. In particular, since there is no passive resistive element, this resonance may create oscillations in the system at the resonance frequency

$$f_{res} = \frac{1}{2\pi\sqrt{\frac{L_\sigma L_f C_f}{L_\sigma + L_f}}}, \tag{1}$$

whenever connected to the machine. Here we used $L_\sigma := \sigma L_s$, the total leakage inductance, as the equivalent *harmonic model* of the induction machine at frequencies higher than the fundamental one. This resonance may also cause drastic deterioration in the performance of any underlying controller being used. This is because the control relies on the measured signals to generate corrective actions, and these signals would be tainted with unwanted oscillations, if the filter resonance is left undamped. Therefore, one would need to create an extra 'outer loop' that takes these oscillations into account and injects an artificial damping into the closed-loop system.

C. Harmonic Model

The harmonic model L_σ of the induction machine is valid for frequencies higher than the fundamental frequency, including the resonant frequency of the filter. Using this harmonic

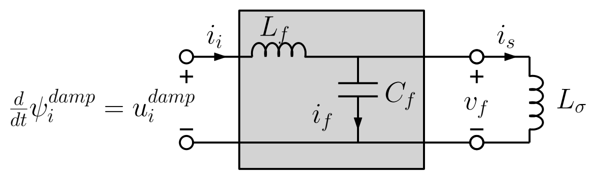

Fig. 5: Harmonic model including the *LC*-filter and the total leakage inductance of the machine L_σ

model, one can write the state-space model of the system consisting of the filter and the machine in the *xy*-plane as

$$\frac{d}{dt}\begin{bmatrix}\bar{i}_i\\ \bar{v}_f\\ \bar{i}_s\end{bmatrix} = \underbrace{\begin{bmatrix}0 & \frac{-1}{L_f}I & 0\\ \frac{1}{C_f}I & 0 & \frac{-1}{C_f}I\\ 0 & \frac{1}{L_\sigma}I & 0\end{bmatrix}}_{A}\underbrace{\begin{bmatrix}\bar{i}_i\\ \bar{v}_f\\ \bar{i}_s\end{bmatrix}}_{\bar{x}} + \underbrace{\begin{bmatrix}\frac{1}{L_f}I\\ 0\\ 0\end{bmatrix}}_{B} u_i^{damp}, \tag{2}$$

where the state $\bar{x} = \begin{bmatrix}\bar{i}_i^T & \bar{v}_f^T & \bar{i}_s^T\end{bmatrix}^T$ is the *filtered version* of the signals.

III. Active Damping for MP^{3}C

The general structure of our proposed control method is shown in Figure 6. We shall describe in what follows the individual control blocks.

A. Active Damping

1) Filtering: The system model (2) used in the LQR-based active damping method relies on the filtered version of the measured state $x = \begin{bmatrix}i_i^T & v_f^T & i_s^T\end{bmatrix}^T$. The filtering is performed in order to extract the harmonic content of the signals close to the resonant frequency f_{res} in (1). As such, the LQR controller would mainly target the frequency content of the signals around the resonant frequency.

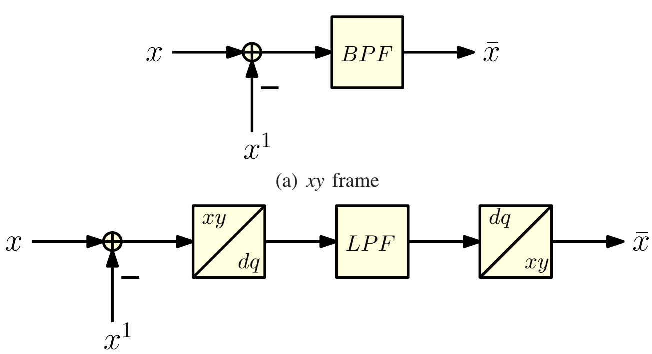

(a) *xy* frame

(b) *dq* frame

Fig. 7: Filtering of the state

There are many different alternatives of filtering the state $x = \begin{bmatrix}i_i^T & v_f^T & i_s^T\end{bmatrix}^T$, two of which are shown in Figure 7. We can either filter the state in the *xy* frame or in the *dq* frame, as shown in Figures 7(a) and 7(b), respectively. In either case, we first extract the harmonic content of the state via subtracting an estimate of the fundamental component, i.e., $y - y^1$. Then, we can apply a bandpass filter (BPF) if we are filtering in the *xy* frame, or a low pass filter (LPF) if we are filtering in the *dq* frame. In this paper, we have chosen to filter the state in the *xy* frame, and the frequency response of the utilized BPF is shown in Figure 8.

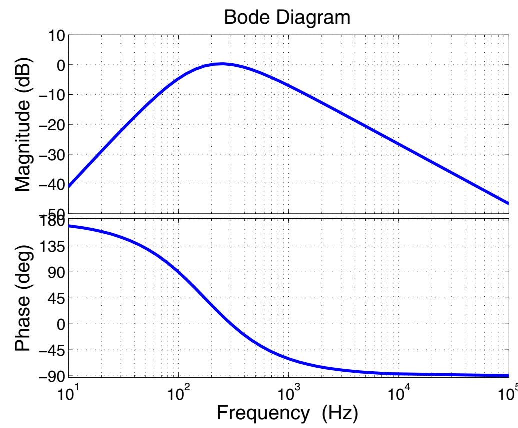

Fig. 8: Bode plot of the BPF

2) LQR Controller: The LQR controller to be designed for active damping relies on a system model (2), as shown in Figure 5. Using (2), we define the associated quadratic objective function to be minimized

$$\mathscr{L} = \int \left(\bar{x}^T Q \bar{x} + (u_i^{damp})^T R u_i^{damp}\right) dt, \tag{3}$$

where $Q = Q^T \geq 0$ is a symmetric positive semidefinite matrix, and $R = R^T > 0$ is a symmetric positive definite matrix. In general, if the pair (A, B) is controllable and the pair $(A, Q^{1/2})$ is observable[1], then the optimal control input is given by

$$u_i^{damp} = -K_{LQR}\bar{x} = -R^{-1}B^T P \bar{x}, \tag{4}$$

where the matrix P is positive-definite symmetric and solves the algebraic Riccati equation $0 = A^T P + PA + Q - PBR^{-1}B^T P$. Therefore, u_i^{damp} is the optimal input to achieve the damping of oscillations in the system due to the resonant filter. One can easily compute the corresponding needed flux to damp the oscillations in the system, given by

$$\psi_i^{damp} = \int u_i^{damp}(\tau) d\tau, \tag{5}$$

This resulting flux will be used in by the MP3C controller, in order to adjust the flux reference and achieve the desired damping of the resonance. Note that in our implementation we have chosen a discrete-time approximation of (5) given by

$$\psi_i^{damp} = T_s u_i^{damp}, \tag{6}$$

where T_s is the sampling period.

[1] The conditions may be relaxed to stabilizability and detectability.

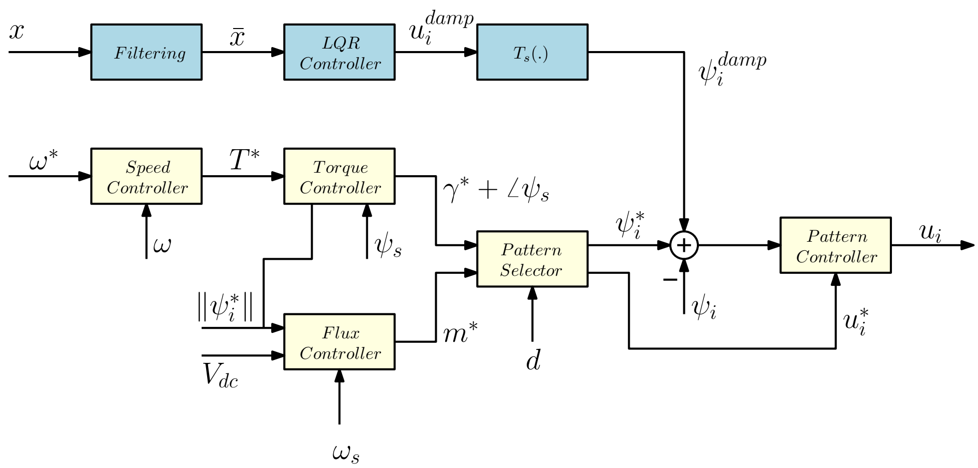

Fig. 6: Complete structure of the controller: MP^{3}C (yellow) with Active Damping (light blue)

B. MP^{3}C with Active Damping

Inherent to the MP^{3}C mechanism is a core online functionality that compares the (estimated) flux ψ to the reference trajectory ψ^* that is generated from the offline-computed OPPs and issues corrective actions. In particular, the original MP^{3}C method in [3] compared the stator flux estimate ψ_s with the reference trajectory ψ_s^*. However, in the presence of an *LC* filter, we only have access to the inverter flux ψ_i and the stator flux ψ_s.

1) Torque Controller: The torque controller receives a desired torque reference T^* from the speed controller, as well as the desired inverter flux reference magnitude $\|\psi_i^*\|$ and the stator flux estimate ψ_s. Using this data, the torque controller computes the reference load angle γ^* of the inverter flux vector ψ_i^* via a steady state phasor analysis of the machine and the filter. Since the controller is designed in the *xy*-frame, the torque controller then issues the flux reference angle $\angle\psi_s + \gamma^*$.[2]

2) Flux Controller: The flux controller issues the desired modulation index to be sent down to the Pattern Selector module using the following formula

$$m^* = \frac{\omega_s \|\psi_i^*\|}{V_{dc}}. \tag{7}$$

3) Pattern Selector: The Pattern Selector receives the desired pulse number d, desired modulation index m^* and the desired angle $\angle\psi_s + \gamma^*$. Based on this data it reads out from a look up table the desired flux reference ψ_i^* and the corresponding optimal switching inputs u_i^*. Consequently, the flux error resulting from the AD loop, the Pattern Selector and the flux estimate is computed as

$$\psi_{i,\text{err}} = \psi_i^* + \psi_i^{damp} - \psi_i, \tag{8}$$

and passed to the Pattern Controller. The vectors used to construct the flux error are depicted in Figure 9.

[2]The PLL is synchronized to the stator flux vector ψ_s.

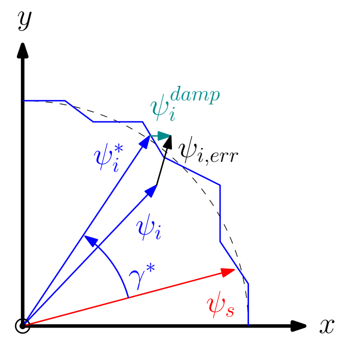

Fig. 9: Given ψ_s, ψ_i^* is read out based on the required load angle γ^*. The flux required for damping ψ_i^{damp} is added to ψ_i^* to construct the required flux vector. Accordingly, the flux error $\psi_{i,err} = \psi_i^* + \psi_i^{damp} - \psi_i$ is obtained.

4) Pattern Controller: This block comprises the online correction mechanism of the offline-computed OPPs. The MP^{3}C control problem can be formulated as an optimization problem with a quadratic objective function and linear constraints, the so called quadratic program (QP). The objective function penalizes both the uncorrected flux error (the controlled variable) and the changes of the switching instants (the manipulated variable), using the diagonal positive-definite weight matrix $W > 0$, whose components are very small. Specifically, the QP is formulated as

$$\begin{aligned} \min_{\Delta t} \quad & J(\Delta t) = \|\psi_{i,\text{err}} - \psi_{i,\text{corr}}(\Delta t)\|^2 + \Delta t^T W \Delta t \\ \text{s. t.} \quad & kT_s \le t_{a1} \le t_{a2} \le \ldots \le t_{an_a} \le t^*_{a(n_a+1)} \\ & kT_s \le t_{b1} \le t_{b2} \le \ldots \le t_{bn_b} \le t^*_{b(n_b+1)} \\ & kT_s \le t_{c1} \le t_{c2} \le \ldots \le t_{cn_c} \le t^*_{c(n_c+1)} \end{aligned} \tag{9}$$

As defined before, $\psi_{i,\text{err}}$ is the inverter flux error in stationary coordinates *xy* and $\psi_{i,\text{corr}}(\Delta t)$ is the correction of the stator flux. The corrections of switching instants are aggregated in the vector $\Delta t = [\Delta t_{a1}\ \Delta t_{a2} \ldots \Delta t_{an_a}\ \Delta t_{b1} \ldots \Delta t_{bn_b}\ \Delta t_{c1} \ldots \Delta t_{cn_c}]^T$. The optimization problem (9) is solved every sampling period T_s. Subsequently, the switching transitions that will occur within the sampling interval are utilized, and the resulting switching commands are sent to the gate units of the semiconductor switches in the inverter. In this paper, we have used a reduced version of the QP (9), the so-called *deadbeat* (DB) version of MP^{3}C. More specifically, the DB version comprises setting the weight matrix W to zero, and defining the optimization horizon as the minimum time interval starting at the current time instant, such that at least two phases exhibit switching transitions. As such, the underlying QP problem reduces to a simple projection operation onto the two phases that exhibit the switching transitions [3].

IV. Simulation Results

As a case study, consider a three-level NPC voltage source inverter (VSI) driving an induction machine (IM) with a constant mechanical load via an *LC* filter, as shown in Figure 3. A 3.3-kV and 50-Hz squirrel-cage IM rated at 2 MVA with a total leakage inductance of 0.25 pu is used as an example of a typical medium-voltage IM. The detailed parameters of the machine, the *LC* filter, and the inverter are summarized in Table II. The per unit system is established using the normalizing quantities $V_N = \sqrt{2/3}V_{rat} = 2694$ V, $I_N = \sqrt{2}I_{rat} = 503.5$ A, and $f_N = f_{rat} = 50$ Hz.

TABLE II: Drive Rated Quantities and Parameters

Machine	V_{rat}	3300 V	R_s	57.8 mΩ
	I_{rat}	356 A	R_r	48.7 mΩ
	P_{rat}	1.587 MW	L_s	42.56 mH
	S_{rat}	2.035 MVA	L_r	41.89 mH
	f_{rat}	50 Hz	L_m	40.01 mH
	n_{rat}	596 rpm		
LC Filter	L_f	2 mH	C_f	200 μF
Inverter	V_{dc}	5200 V	C_{dc}	7 mF

A. Steady State Operation without the LC Filter

We simulated the system above without including the *LC* filter, i.e., $L_f = 0$ and $C_f = 0$. Accordingly, the AD loop was deactivated. We used pulse number $d = 8$ at rated speed of 1 pu and rated torque of 1 pu. The stator current, stator current spectrum, torque, and switch positions are shown in Figure 10(a) through 10(d), respectively. The resulting THD of the stator current is 2.95%.

B. Steady State Operation with the LC Filter and Active Damping

We simulated the system again with the *LC* filter in Table II and turned on the AD loop. We used pulse number $d = 8$ at rated speed of 1 pu and rated torque of 1 pu. The LQR gain was designed for a choice of the weight matrices $Q = \begin{bmatrix} 0.2I & 0 & 0 \\ 0 & I & 0 \\ 0 & 0 & I \end{bmatrix}$ and $R = 0.1I$. The damping flux ψ_i^{damp} was implemented at discrete sampling interval of $T_s = 25\mu$s

$$\psi_i^{damp}(k) = T_s u_i^{damp}(k) = -T_s K_{LQR} \begin{bmatrix} i_i(k) \\ v_f(k) \\ i_s(k) \end{bmatrix}, \qquad (10)$$

where

$$K_{LQR} = \begin{bmatrix} 2.0315I & 3.3765I & 1.1959I \end{bmatrix},$$

and the signals were filtered using a third order BPf depicted in Figure 8. The stator current, stator current spectrum, torque, and switch positions are shown in Figure 11(a) through 11(d), respectively. The resulting stator current THD was reduced to 0.71%. It is important to note the difference in the state current spectrum between Figures 10(b) and 11(b); the harmonic content beyond and including the 11^{th} harmonic has been drastically attenuated by the filter. However, the content of the 5^{th} and 7^{th} harmonics has been slightly amplified; this is due to the fact that the resonance frequency is around 304 Hz in our setup.

C. Steady State Operation with the LC Filter, Active Damping, and Harmonic Elimination

In order to alleviate the effects of the harmonic content of the OPP around the filter resonance frequency, we computed new OPPs in which the 5^{th}, 7^{th}, 11^{th}, and 13^{th} harmonics were eliminated. Except for the new OPPs, the simulation setup was kept exactly the same as in the last case. The stator current, stator current spectrum, torque, and switch positions are shown in Figure 12(a) through 12(d), respectively. Note that the content of the 5^{th} and 7^{th} harmonics has been reduced by almost 50%, as seen when comparing Figures 11(b) and 12(b). The current THD was further reduced to 0.45%. Finally, the switching frequency in all three scenarios was around 400 Hz.

TABLE III: Current THD and Harmonic Content for All Three Scenarios

	No *LC* Filter	*LC* filter	*LC* filter and HE
THD	2.95%	0.71%	0.45%
5^{th}	0.3%	0.37%	0.17%
7^{th}	0.05%	0.59%	0.41%

V. Conclusions

We proposed a new method of damping unwanted oscillations due to a resonant *LC* output filter in medium voltage drives. The method is based on LQR theory and provides corrective actions to the flux error signals, which are in turn used by the Model Predictive Pulse Pattern Controller to generate the control signals. The results are validated via numerical simulations. Future work will focus on advanced methods of achieving active damping via direct manipuation of the switch positions.

References

[1] G. S. Buja. Optimum output waveforms in PWM inverters. *IEEE Trans. Ind. Appl.*, 16(6):830–836, Nov./Dec. 1980.

[2] J. Dannehl, F. W. Fuchs, S. Hansen, and P. Thorgersen. Investigation of active damping approaches for PI-based current control of grid-connected pulse width modulation converters with LCL filters. *IEEE Trans. Ind. Appl.*, 46(4):1509–1517, Jul./Aug. 2010.

[3] T. Geyer, N. Oikonomou, G. Papafotiou, and F. Kieferndorf. Model predictive pulse pattern control. *IEEE Trans. Ind. Appl.*, 48(2):663–676, Mar./Apr. 2012.

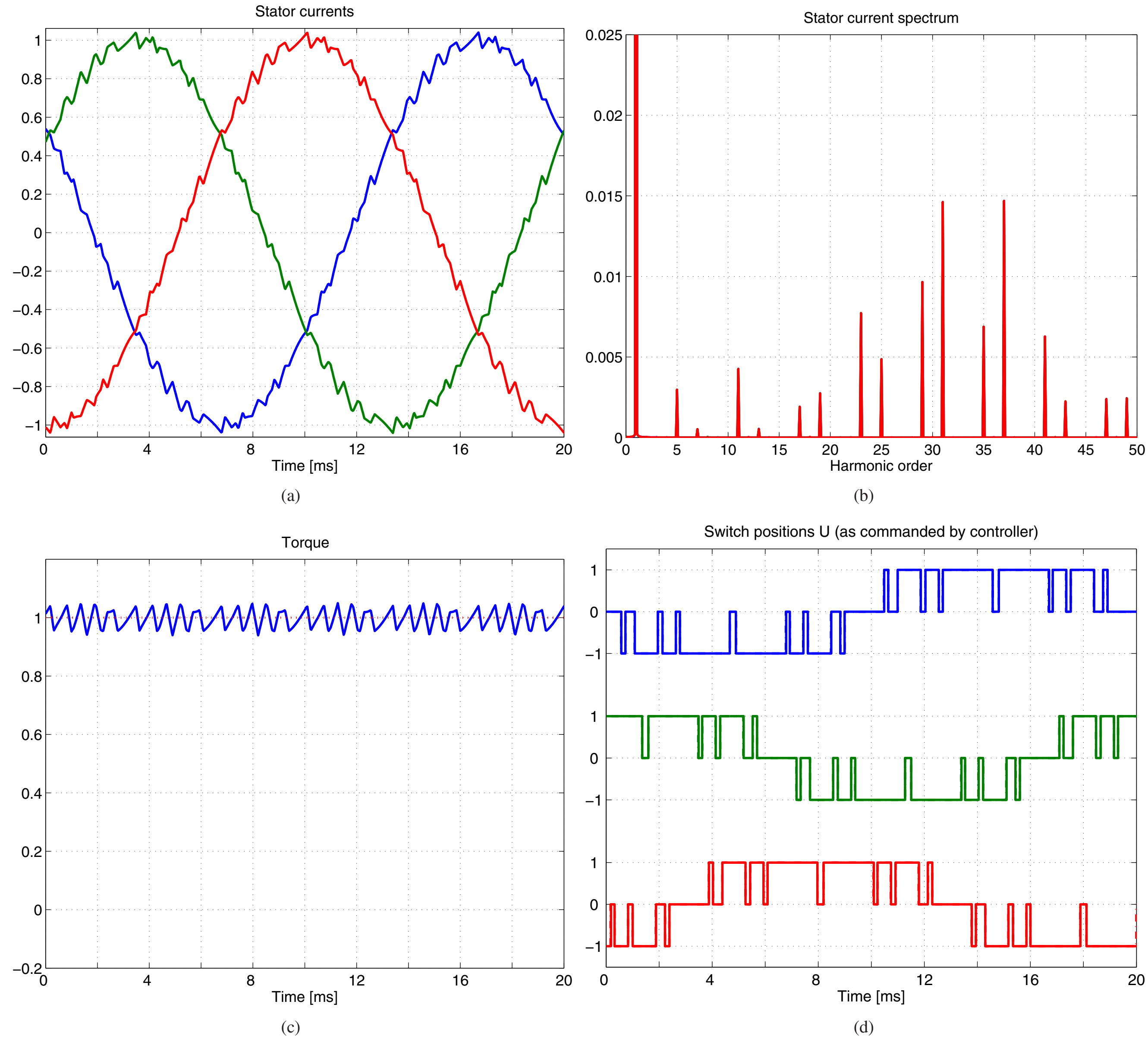

Fig. 10: MP^{3}C without active damping, when the machine is connected directly to the inverter.

[4] M. Malinowski and S. Bernet. A simple voltage sensorless active damping scheme for three-phase PWM converters with an LCL filter. *IEEE Trans. Industrial Electronics*, 55(4):1876–1880, Apr. 2008.

[5] S. Mastellone, G. Papafotiou, and T. Geyer. Predictive harmnonics and resonances compensation for MV drives. EP-2546979-A1, Mar. 2009.

[6] N. Oikonomou, C. Gutscher, P. Karamanakos, F. Kieferndorf, and T. Geyer. Model predictive pulse pattern control for the five-level active neutral point clamped inverter. *IEEE Trans. Ind. Appl.*, 49(6):2583–2592, 2013.

[7] P. Pahjolainen and C. Stulz. Method and apparatus for direct torque control of a three-phase machine. United States Patent 5734249, Mar. 1998.

[8] A. Sapin, P. Steimer, and J.-J. Simond. Modeling, simulation, and test of a three-level voltage-source inverter with output *LC* filter and direct torque control. *Proc. IEEE Ind. Appl. Soc. Annu. Mtg.*, 43(2):469–475, Mar./Apr. 2007.

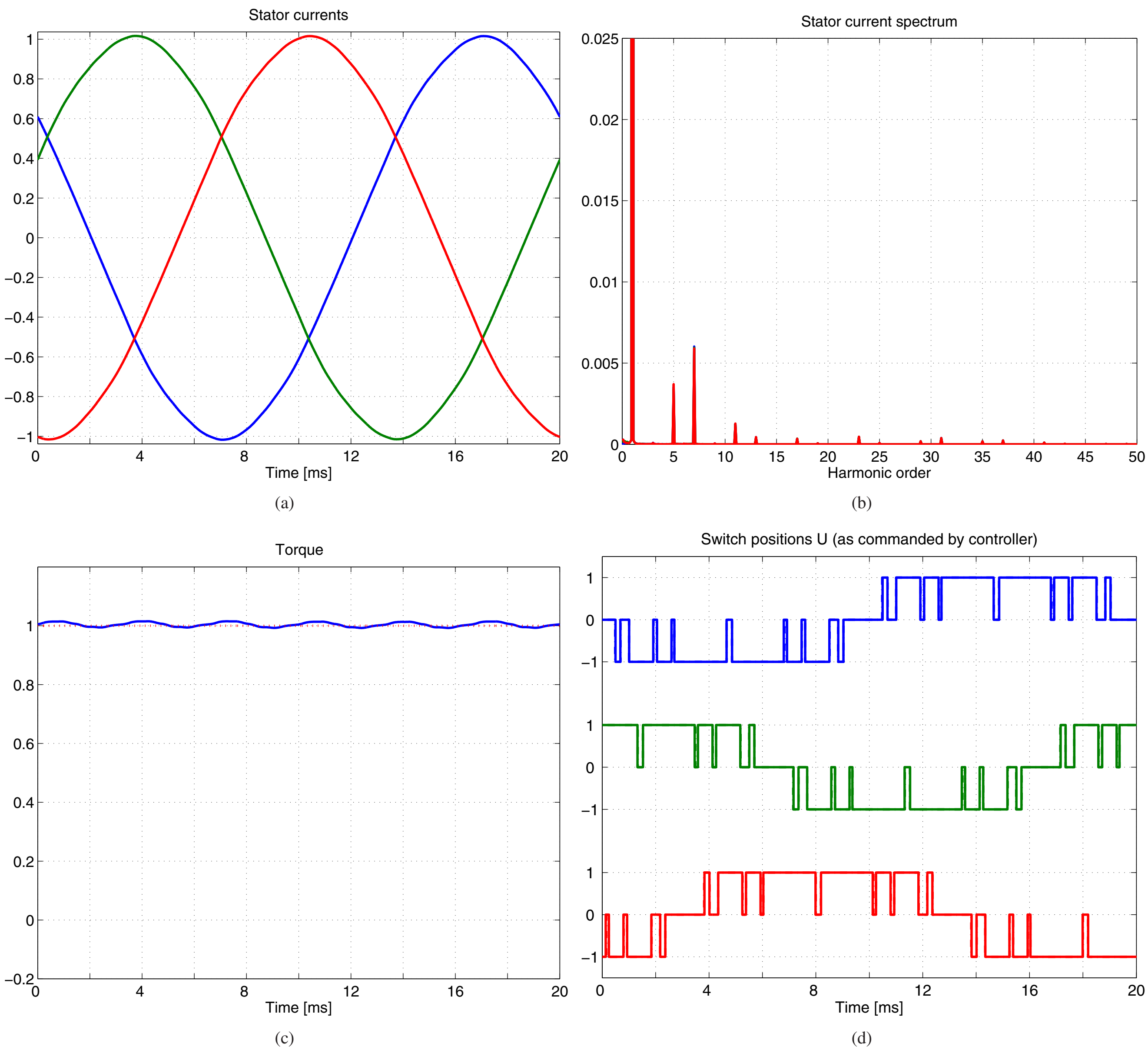

(a) (b) (c) (d)

Fig. 11: MP^{3}C with active damping

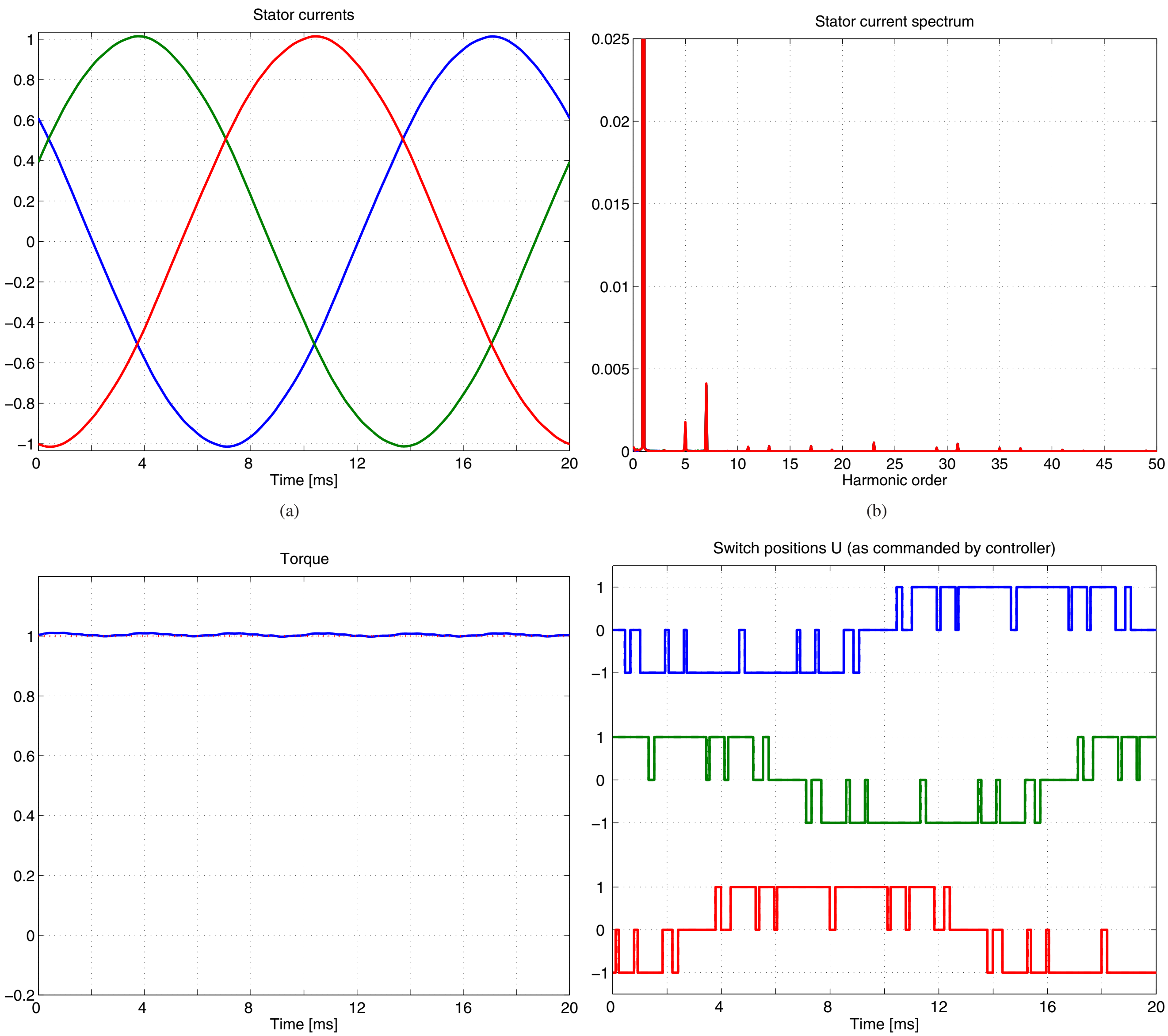

Fig. 12: MP^{3}C with active damping and elimination of the 5^{th}, 7^{th}, 11^{th}, and 13^{th} harmonics from the OPP